AIAA JOURNAL
Vol. 40, No. 8, August 2002

Prediction of Residual Strength and Curvilinear Crack Growth in Aircraft Fuselages

Chuin-Shan Chen*
National Taiwan University, Taipei 10617, Taiwan, Republic of China
and
Paul A. Wawrzynek† and Anthony R. Ingraffea‡
Cornell University, Ithaca, New York 14853

Two practical engineering approaches to assess the structural integrity of aircraft fuselages are presented. Both approaches combine fracture mechanics with thin-shell finite element analyses to predict structural responses quantitatively. The first approach uses the crack-tip opening angle fracture criterion to predict residual strength of KC-135 fuselages. The second approach uses T-stress and fracture toughness orthotropy to predict crack-growth trajectory in narrow-body fuselages. For residual strength prediction 12 damage scenarios, which might occur in applications, are examined. It is found that the model with small multiple-site cracking and material thinning caused by corrosion damage has the worst load-carrying capacity. For curvilinear crack-growth simulation a directional criterion based on the maximum tangential stress theory accounting for the effect of T-stress and fracture toughness orthotropy is used to predict crack-growth trajectory. Both T-stress and fracture toughness orthotropy are found to be essential to predict the observed crack path, where the trajectory experiences crack turning and flapping phenomena.

I. Introduction

CONCERN about residual strength of aging aircraft prompted the development of an advanced analysis toolkit for fatigue and fracture problems.[1] One component of the toolkit FRANC3D/STAGS has been developed to assess damage tolerance in critical aircraft structures.[2,3] The program is capable of tracking crack growth using FRANC3D[4] and performing nonlinear thin-shell analysis using STAGS.[5] This paper presents two recent studies on simulating crack growth in airplane fuselages using the FRANC3D/STAGS program. The software program FRANC3D is available from the Cornell Fracture Group's web site at www.cfg.cornell.edu. Animations of stable crack growth and plastic zone evolution in the KC-135 fuselage panel and curvilinear crack growth in the narrow-body fuselage panel are also available from the web site.

The first example is residual strength prediction for a typical KC-135 fuselage panel.[6] The crack-tip opening angle (CTOA) fracture criterion[7] and elastic-plastic thin-shell finite element analysis are used to characterize stable crack growth and predict residual strength. The objective of this study is to examine several damage scenarios that might occur in pressurized fuselages and their effects on residual strength prediction. In particular, lead crack growth, presence of multiple-site damage (MSD) from rivet holes, multiple crack interaction, and material loss as a result of corrosion damage are studied.

The second example is curvilinear fatigue crack-growth simulation in a generic narrow-body fuselage. This is related to the growing interest by using crack turning phenomenon to improve the structural integrity of aircraft structures.[8–10] A reliable crack trajectory prediction for fatigue and fracture thus serves as a crucial step to use this evolving methodology. In this study linear elastic fracture mechanics (LEFM) parameters including stress intensity factors and T-stress, together with orthotropy of fracture toughness, are used to predict the direction of fatigue crack growth. The objective is to study the effects of various fracture parameters on crack-growth trajectory prediction and validate the analysis methodology by comparing with experimental observations.

Received 12 December 2000; revision received 24 February 2002; accepted for publication 1 March 2002. Copyright © 2002 by the American Institute of Aeronautics and Astronautics, Inc. All rights reserved. Copies of this paper may be made for personal or internal use, on condition that the copier pay the $10.00 per-copy fee to the Copyright Clearance Center, Inc., 222 Rosewood Drive, Danvers, MA 01923; include the code 0001-1452/02 $10.00 in correspondence with the CCC.

*Assistant Professor, Department of Civil Engineering, No. 1, Section 4, Roosevelt Road.
†Senior Research Associate, Cornell Fracture Group, 641 Rhodes Hall.
‡Dwight C. Baum Professor of Engineering, School of Civil and Environmental Engineering.

II. Residual Strength Prediction of KC-135 Fuselage

A crown lap-jointed KC-135 fuselage panel is chosen for analysis. This is a three-stringer-wide, three-frame-long, fuselage panel. The panel section has a radius of curvature of 72 in. (1829 mm). It contains a lap joint at the central stringer. The lap joint is a typical three-row configuration with $\frac{3}{16}$-in. (4.76-mm)-diam countersunk-head rivets. The other two stringers are spot-welded to the skin. The upper and lower skins are 0.04-in. (1.02-mm)-thick, 2024-T3 aluminum alloy. The stringers and frames are 7075-T6 aluminum alloy. Frames are connected to stringers by rivets. The panel configurations are shown in Figs. 1 and 2. The frame and stringer dimensions are shown in Fig. 3.

A. Numerical Model

All structural components including skins, stringers, and frames are modeled by shell elements. A piecewise linear representation is used for the uniaxial stress-strain curves for 2024-T3 and 7075-T6 aluminum alloys (see Figs. 4 and 5). Symmetric boundary conditions are imposed on all of the boundary edges to simulate a cylinderlike fuselage structure. Pressure loading is applied on all of the external skins. Both geometric and material nonlinearities are included in the analysis.

Rivets are modeled by one-dimensional elastic-plastic fastener elements that connect shell finite element nodes in the upper and lower skins. Each fastener element has six degrees of freedom, corresponding to extension, two shearing, two bending and twisting of the rivet. The stiffness of each degree of freedom is defined by prescribing a force-deflection curve. The axial, flexural, and torsional stiffnesses are computed by assuming that the rivet behaves like a simple elastic rod with a diameter of $\frac{3}{16}$ in. (4.76 mm). The elastic shear stiffness of the fastener element is computed by the following empirical relation developed by Swift[11]:

$$K_{\text{rivet}} = \frac{ED}{[A + C(D/t_1 + D/t_2)]} \tag{1}$$

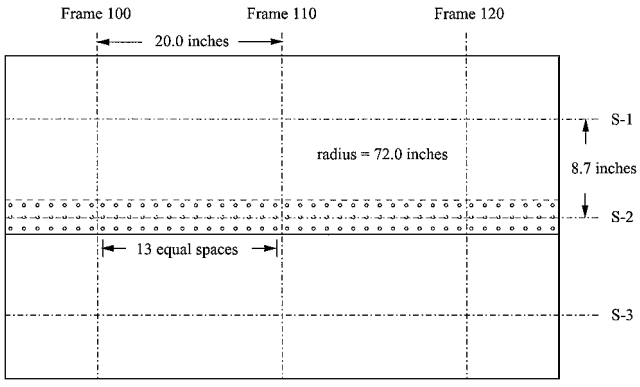

Fig. 1 Dimensions of the KC-135 fuselage panel.

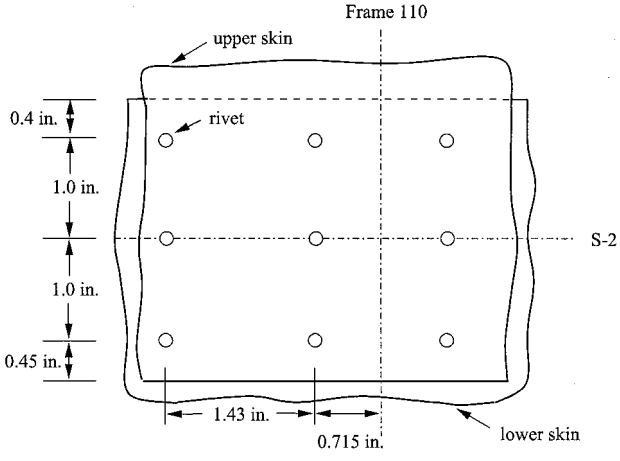

Fig. 2 Detailed rivet spacing for the KC-135 fuselage panel.

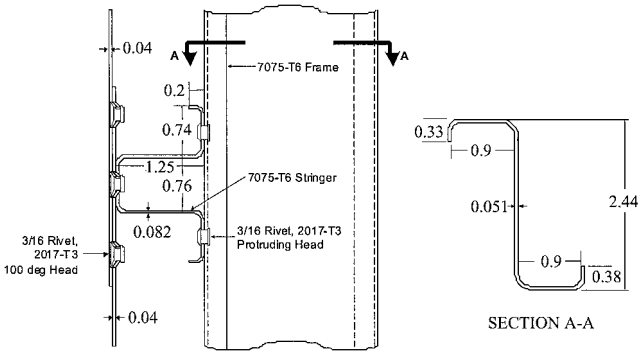

Fig. 3 Dimensions of stringer and frame for the KC-135 fuselage panel (dimensions in inches; 1 in. = 25.4 mm; modified after Ref. 6).

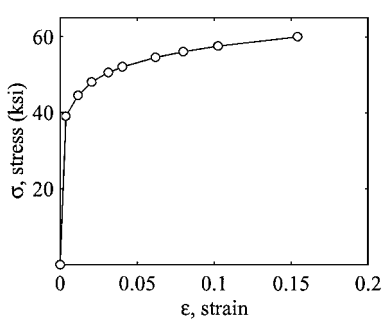

stress (ksi)	strain
0.0	0.0
39.0	0.003714
44.5	0.01172
48.0	0.02052
50.5	0.03131
52.0	0.04047
54.5	0.06199
56.0	0.07985
57.5	0.10254
60.0	0.15427

E = 1.05e+04 ksi
ν = 0.33

Fig. 4 KC-135 fuselage panel: piecewise linear representation of the uniaxial stress-strain curve for 2024-T3 aluminum.

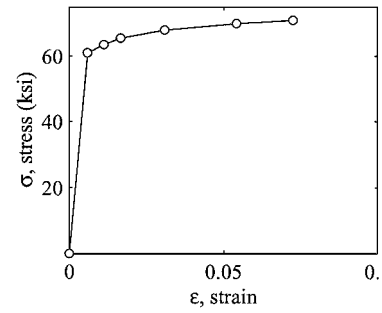

stress (ksi)	strain
0.0	0.0
61.0	0.00593
63.5	0.0112
65.5	0.01664
68.0	0.03093
70.0	0.05419
71.0	0.07257

E = 1.03e+04 ksi
ν = 0.33

Fig. 5 KC-135 fuselage panel: piecewise linear representation of the uniaxial stress-strain curve for 7075-T6 aluminum.

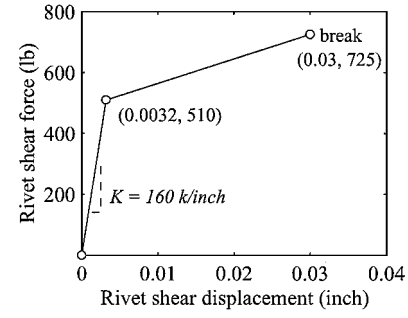

Fig. 6 KC-135 fuselage panel: rivet shear stiffness and strength.

where E is the elastic modulus of the sheet material, D is the rivet diameter, t_1 and t_2 are the thicknesses of the joined sheets, and A and C are empirical constants, which equal to 5 and 0.8 for aluminum rivets. The initial shear yielding and ultimate shear strength of the rivets are assumed to occur at load levels of 510 lb (2268 N) and 725 lb (3225 N), respectively. A 50% reduction of the shear stiffness is assumed after the initial yielding. Once the fastener reaches its ultimate strength, it breaks and loses its load-carrying capacity. The shearing force-deflection curve is shown in Fig. 6.

B. Fracture Criterion and Crack Configurations

The critical crack-tip opening angle ($CTOA_c$) is used to characterize elastic-plastic crack growth and to predict residual strength. The CTOA fracture criterion asserts that the angle maintains a constant value during stable crack growth for a given thickness of a metallic material. Previous studies of residual strength prediction using two-dimensional elastic-plastic analyses had mixed success.[7] Typically, the predicted residual strength would agree with test results up to a certain width of the panels. The discrepancy between two-dimensional predictions and test results for larger panels was thought to be related to the three-dimensional constraint effects. Although thin-sheet structures behave essentially in plane stress, the constraint from the finite thickness of the specimens can cause the regions, local to the crack tip, to approach plane-strain conditions.[12–14]

Extensive numerical studies of two- and three-dimensional elastic-plastic fracture have been conducted to investigate the constraint effects on residual strength prediction.[13,15–17] From these comes the concept of a plane-strain core, which assumes that for thin-sheet structures a small near-tip region reaches plane-strain conditions whereas the rest of the structural behaves essentially in plane stress. This concluded that, although three-dimensional simulations are best to quantify the constraint effects, two-dimensional simulations with the plane-strain core concept seem to capture the effects for residual strength prediction.

For two-dimensional and thin-shell problems the width and the height define the plane-strain core region (Fig. 7). Although the height of the plane-strain core has a modest effect on residual strength prediction, the width of the plane-strain core has a relatively minor influence.[18] The plane-strain core concept is used for all analyses presented here.

Table 1 Initial crack configuration for KC-135 model

Model	Lead crack length	MSD crack length[a]
1	7.14 in. (181.36 mm)	None
2	7.14 in. (181.36 mm)	0.025 in. (0.64 mm)
3	7.14 in. (181.36 mm)	0.046 in. (1.17 mm)
4	10.0 in. (254 mm)	None
5	10.0 in. (254 mm)	0.025 in. (0.64 mm)
6	10.0 in. (254 mm)	0.046 in. (1.17 mm)

[a]Emanating from both sides of a fastener hole.

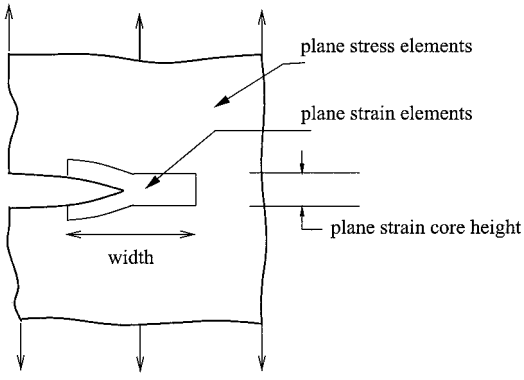

Fig. 7 Schematic of the plane-strain core concept.

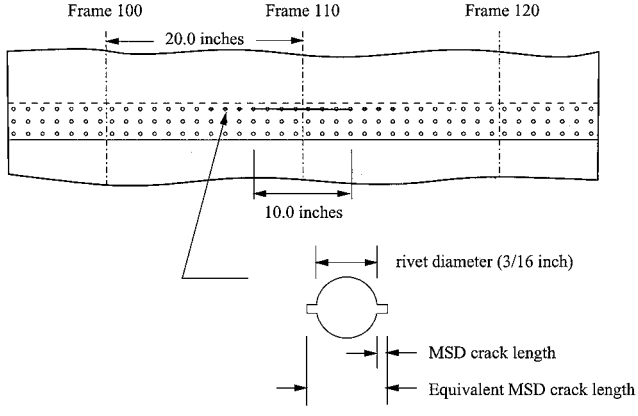

Fig. 8 Crack configurations with a 10-in. (254-mm) initial lead crack and MSD (external view).

The $CTOA_c$ that is used is 5.7 deg, measured 0.04 in. (1.02 mm) behind the crack tip, with a plane-strain core height equal to 0.08 in. (2.03 mm). No experimental crack-growth data are available to date for this material and thickness; this particular $CTOA_c$ value is estimated based on the 5.25 deg used in 0.09-in. (2.29-mm)-thick, 2024-T3 bare material used in Refs. 17 and 19. The plane-strain core height is assumed to be twice the sheet thickness. Six different crack configurations with various lengths of lead and MSD cracks are studied. The initial configurations prior to crack growth are shown in Table 1.

The lead crack is located symmetrically about the central frame line. The MSD pattern is symmetric about the lead crack at the three rivets in front of the lead crack. The lead and MSD cracks are located along the upper rivet row in the upper skin of the joint. The crack configurations with a 10-in. (254-mm) initial lead crack are shown in Fig. 8. Because rivet holes are not modeled explicitly in the finite element model, a small crack with a length equal to the rivet diameter plus the MSD length is used to model the MSD crack.

A mesh pattern with 0.04-in. (1.02-mm) crack-tip elements is used. This pattern is similar to the one used in the flat-panel simulation reported in Refs. 16 and 19. A finite element mesh for the model is shown in Figs. 9 and 10. In addition to the effects of MSD, material thinning as a result of corrosion damage is also studied.

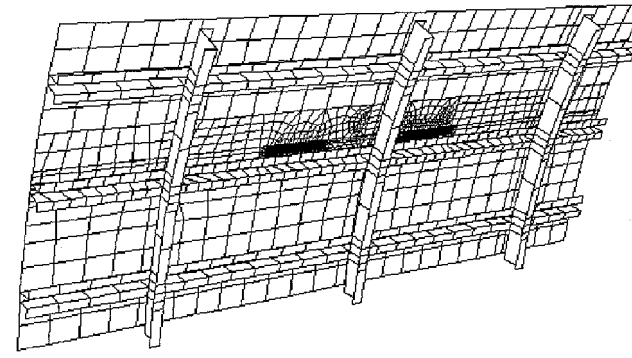

Fig. 9 Finite element mesh for the KC-135 fuselage panel.

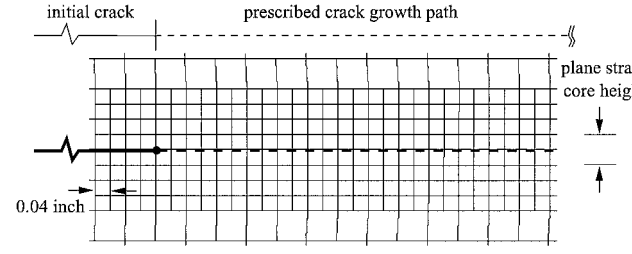

Fig. 10 Detailed mesh around crack path for the KC-135 fuselage panel.

The effect of material thinning is modeled by a uniform reduction in thickness of the upper skin at the lap joint in the two center bays.

C. Numerical Results and Discussion

Figure 11 shows the predicted results of the operating pressure loading vs the total crack extension for all of the cases conducted in this study. Predicted residual strengths summarized in Fig. 12 indicate the following:

1) The MSD cracks significantly reduce the residual strength of the fuselage panel. A 21.8 to 28.0% loss of residual strength as a result of the presence of small MSD is observed.

2) A 10% uniform thickness degradation caused by corrosion damage reduces the residual strength by 3.4 to 9.0%. The coupling of MSD and corrosion damage leads to the most severe damage scenario.

3) In general, increasing the lead and MSD crack lengths reduces the residual strength. However, for the cases with a 10-in. (254-mm) initial lead crack residual strength seems to be relatively insensitive to the MSD crack sizes, similar to the conclusions drawn in Ref. 20.

4) The required residual strength for the aircraft fuselages is 12.5 psi (86.18 kPa). The predicted residual strength for the MSD and/or corrosion damage cases with a 10-in. (254-mm) initial lead crack is well below the required strength.

The deformed structure at residual strength for the case with a 10-in. (254-mm) initial lead crack but without MSD and corrosion damage is shown in Fig. 13. Out-of-plane bulging is observed in the skin crack edges. Because of the stiffness of the stringer, the bulging at the lower crack edge is much smaller than the opposing side. The unsymmetric out-of-plane bulging leads to an antisymmetric bending deformation field at the crack tips.[21] Figures 14 and 15 depict the predicted plastic zones for the cases with a 10-in. (254-mm) initial lead crack as the panel reaches its residual strength. The plastic zone is composed from those elements with computed effective stresses exceeding the initial yield stress. As shown in Fig. 14, the evolving plastic zones are well-confined by the elastic regions within the frames. For the case without MSD, dominant plastic zones accompanying the lead crack tips are observed. For the case with MSD, plastic zones are developed at the multiple crack tips. The plasticity distributions are highly influenced by the multiple crack interactions; the animation of the plastic zone evolution is available from the Cornell Fracture Group's web site at www.cfg.cornell.edu.

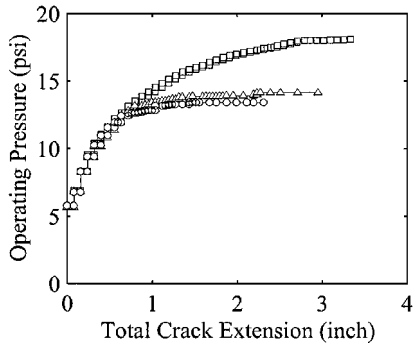

7.14-in. (181.4-mm) initial lead crack

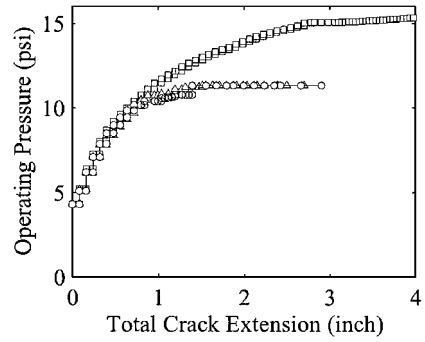

10-in. (254-mm) initial lead crack

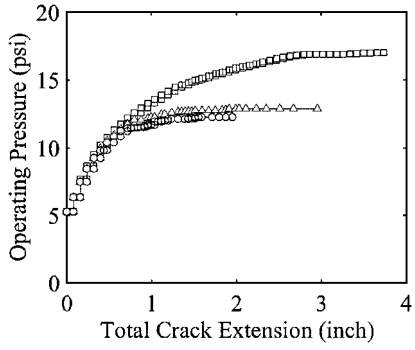

7.14-in. (181.4-mm) initial lead crack with corrosion damage

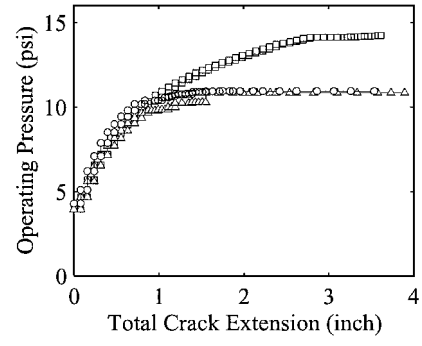

10-in. (254-mm) initial lead crack with corrosion damage

Fig. 11 Predicted operating pressure vs total crack extension for the KC-135 fuselage panel: □, no MSD; △, 0.025-in. (0.64-mm) MSD; and ○, 0.046-in. (1.17-mm) MSD.

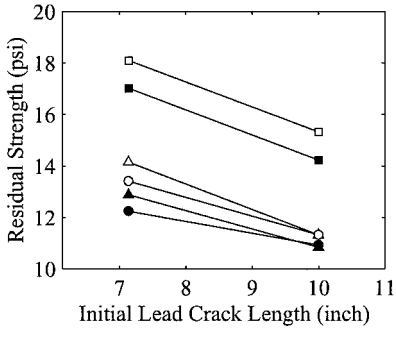

Fig. 12 Predicted residual strength vs initial lead crack length: □, no MSD; △, 0.025-in. (0.64-mm) MSD; ○, 0.046-in. (1.17-mm) MSD; ■, no MSD, corrosion; ▲, 0.025-in. (0.64-mm) MSD, corrosion; ●, 0.046-in. (1.17-mm) MSD, corrosion; and ——, curve fit.

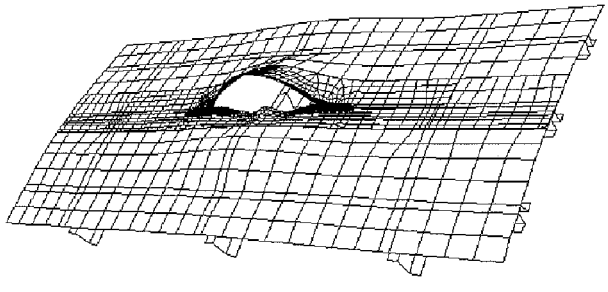

Fig. 13 Deformed shape of the KC-135 fuselage panel [pressure = 15.3 psi (105.5 kPa); magnification factor = 5.0].

III. Curvilinear Crack Growth in a Narrow-Body Fuselage

A. Description of Experiment

A generic narrow-body fuselage panel with tear straps, stringers, stringer clips, and frames was tested by the Boeing Commercial Airplane Group. Skins and tear straps were 0.036-in. (0.91-mm) thick, 2024-T3 clad aluminum alloy. Stringers, frames, and stringer clips were 7075-T6 clad aluminum alloy. The tear straps were hot-bonded

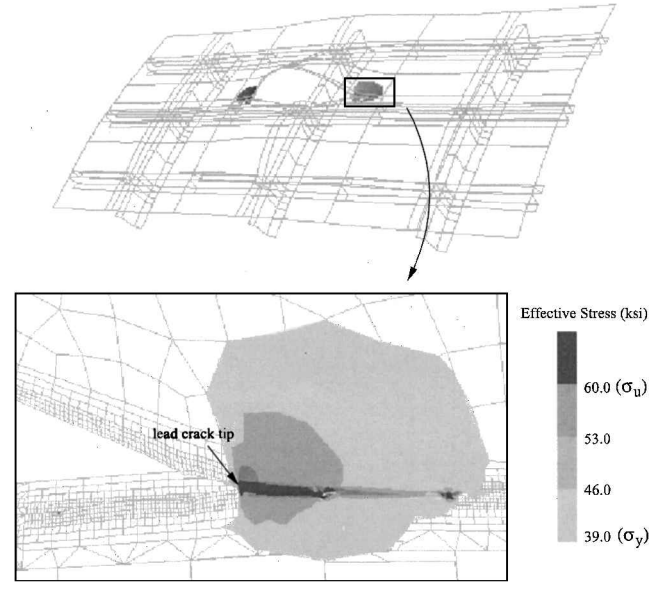

Fig. 14 Predicted plastic zones for 10-in. (254-mm) initial lead crack without MSD [pressure = 15.3 psi (105.5 kPa); magnification factor = 5.0].

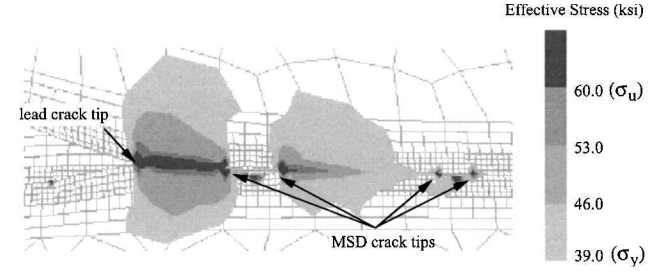

Fig. 15 Predicted plastic zones for 10-in. (254-mm) initial lead crack with 0.025-in. (0.64-mm) MSD [pressure = 11.3 psi (77.9 kPa); magnification factor = 5.0].

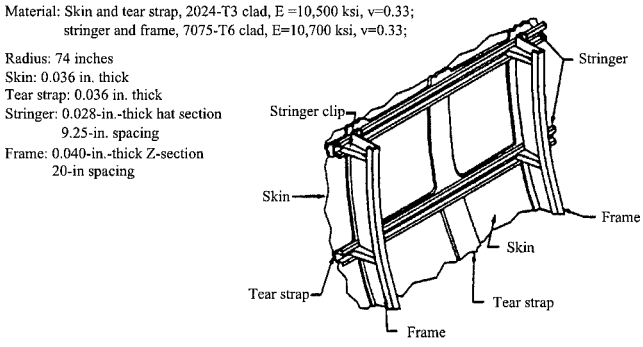

Fig. 16 Structural features of a generic narrow-body fuselage panel (modified after Ref. 9).

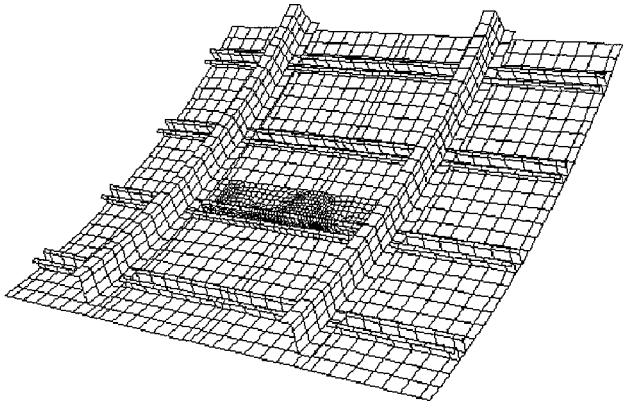

Fig. 17 Finite element model for the generic narrow-body fuselage panel.

to the skins at midbay and at each frame station. The structural features of the test panel are shown in Fig. 16. More information about panel dimensions can be found in Ref. 3 and online at http://www.cfg.cornell.edu.

The tested panel had a 5.0-in. (127-mm) initial saw cut in the transverse-longitudinal orientation centered on the midbay tear strap and just above the stringer tear strap. The saw cut went completely through both the skin and midbay tear strap. The panel was inserted into a test fixture with a radius of curvature of 74 in. (1880 mm) to match narrow-body airplanes. A cyclic pressure of 7.8 psi (53.8 kPa) was applied to propagate the crack. During the test, the positions of the crack tips were recorded. The detailed test data can be found in Ref. 3.

B. Numerical Model

The entire curvilinear crack-growth simulation consists of more than 20 in. (508 mm) of crack extension. As a result, using a global-local hierarchical modeling approach[3] could require continual updating of the boundary conditions from the preceding model in the hierarchy as a result of the crack growth. This would increase efforts substantially in performing the numerical analyses. For this specific problem only internal pressure was applied to the structure; thus, a simple numerical model using symmetric boundary conditions might suffice to simulate the panel test.

In this study a four-stringer-bay wide and two-frame-bay long panel was analyzed. All structural components including skins, stringers, and frames were modeled by quadrilateral shell elements. Each node of the shell element has six degrees of freedom. A typical finite element mesh used in the simulation is shown in Fig. 17.

Geometrically nonlinear analyses are performed. Pressure loading is applied on the skin of the shell model. Symmetric boundary conditions are imposed on all of the boundary edges of the model to simulate a cylinder-like fuselage structure. Uniform axial expansion is allowed at one longitudinal end. On this boundary edge, an axial force equal to $(PR/2)\cdot L$ is assigned, where P is the applied pressure, R is the radius of the panel, and L is the arc length of the edge.

C. Crack-Growth Directional Criteria

Various directional criteria have been proposed. Zaal[22] gives an excellent review of this subject. In the following, the equations used in this study to compute the fatigue crack-growth direction are outlined. Detailed derivations can be found elsewhere.[2]

It is assumed that the crack will start to grow from the tip in the direction perpendicular to which the tangential stress $\sigma_{\theta\theta}$ is maximum. Considering only the singular stresses (or the first-order terms) from the asymptotic expansions, the direction of crack growth or the crack propagation angle θ_c is determined by solving

$$K_{\mathrm{I}}\sin\theta_c + K_{\mathrm{II}}(3\cos\theta_c - 1) = 0 \tag{2}$$

where K_{I} and K_{II} are mode I and mode II stress intensity factors. This criterion was developed by Erdogan and Sih.[23]

If one includes the constant stresses (or the second-order terms) from the asymptotic expansions, the crack propagation angle θ_c is determined by solving

$$\begin{aligned} &1\Big/\sqrt{2\pi r_c}\Big[-\tfrac{3}{4}\cos(\theta_c/2)\Big][K_{\mathrm{I}}\sin\theta_c + K_{\mathrm{II}}(3\cos\theta_c - 1)] \\ &\qquad + 2T\sin\theta_c\cos\theta_c = 0 \\ &1\Big/\sqrt{2\pi r_c}\Big[-\tfrac{3}{8}(3\cos\theta_c - 1)\Big][K_{\mathrm{I}}\cos(\theta_c/2) - K_{\mathrm{II}}\sin(\theta_c/2)] \\ &\qquad + 2T\cos 2\theta_c < 0 \end{aligned} \tag{3}$$

where r_c is a "critical" distance away from the crack tip and T is the constant stress or the T-stress. The physical meaning of r_c has been studied in Ref. 24. The asymptotic stress expansion from the crack tip including the T-stress and other higher-order terms can be found in Ref. 25. This directional criterion was proposed by Williams and Ewing[26] and later corrected by Finnie and Saith.[27] Figure 18 shows the predicted propagation angle with the effect of T-stress. A dimensionless parameter $\bar{T} \equiv \frac{8}{3}(T/K_{\mathrm{I}})\sqrt{(2\pi r_c)}$ used in Ref. 10 is introduced to normalize the T-stress effect.

For crack growth in orthotropic media, it is assumed that the crack propagates in the direction of maximum normalized stress, such that

$$\text{Maximum}\left[\frac{\sigma_{\theta\theta}(K_{\mathrm{I}}, K_{\mathrm{II}}, T, r_c, \theta)}{K_c(\alpha)}\right] = \left(\frac{\sigma_{\theta\theta}}{K_c}\right)_{\text{critical}} \quad \text{at} \quad \theta = \theta_c \tag{4}$$

where α is the angle characterizing the material grain orientation and $K_c(\alpha)$ is the strength parameter characterizing the material fracture resistance.

A simple elliptical function is used to characterize the anisotropic fracture toughness $K_c(\alpha)$ (Refs. 28 and 29), that is,

$$K_c(\alpha) = \sqrt{1\Big/\left[\cos^2\alpha + (1/\bar{K}_m)^2\sin^2\alpha\right]} \tag{5}$$

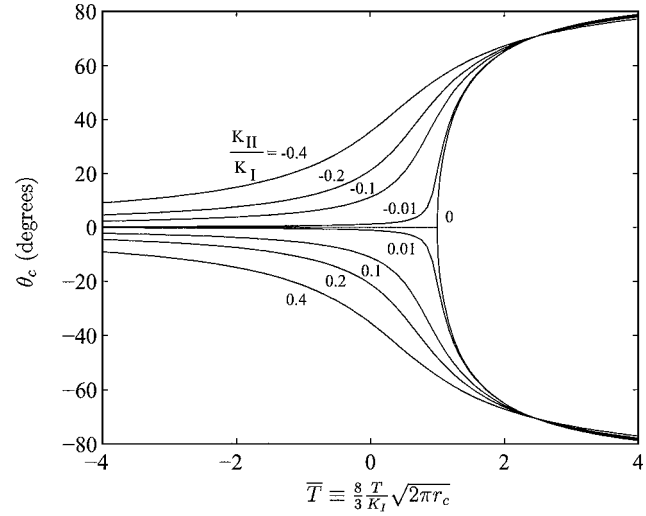

Fig. 18 Predicted propagation angle from the maximum tangential stress theory with T-stress [Eq. (3)].

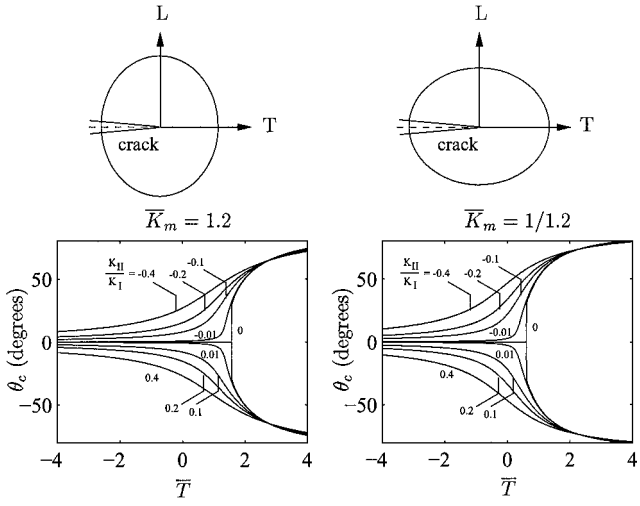

Fig. 19 Effects of fracture orthotropy ratio on predicted propagation angle.

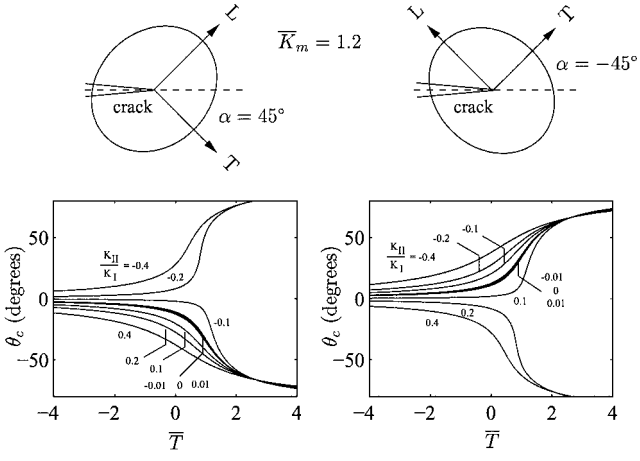

Fig. 20 Effects of material orientation on predicted propagation angle.

where $\bar{K}_m$ is the fracture orthotropy ratio defined as $\bar{K}_m \equiv K_c(T)/K_c(L)$. $K_c(L)$ is the fracture toughness along the material longitudinal (L) direction and $K_c(T)$ is the fracture toughness along the transverse (T) direction.

Both the fracture orthotropy ratio $\bar{K}_m$ and the material orientation angle α can affect the predicted angle of impending fracture propagation θ_c, as demonstrated in Figs. 19 and 20.

D. Fracture Parameter Evaluation

Calculated deformation and stress fields near the crack tip are used to compute fracture parameters for crack-growth simulations. The modified crack closure integral method is used to compute the membrane and bending stress intensity factors (K_1, K_{II}, k_1, k_2).[3,30] A simple displacement correlation method is used to evaluate the T-stress[10,31]. Although a better numerical method for T-stress computation using a path-independent integral is available for two-dimensional models,[26,32] its counterpart for curved shells is not available to date. Using the simple displacement correlation method, a 5–10% error in the computed T-stress is expected. The crack-growth directional criteria, Eqs. (3) and (4) for the isotropic and orthotropic media, are used to predict the propagation angle in thin-shell structures.

E. Numerical Results

1. Effect of T-Stress and r_c

The effect of T-stress and r_c on crack trajectory prediction is studied first. Crack-growth direction is predicted by the isotropic directional criterion [Eq. (3)]. Figure 21 plots the predicted crack trajectories with $r_c = 0$ (T-stress effects ignored) and $r_c = 0.09$ in. (2.29 mm) as well as the experimental measurements. Figure 22 shows the computed deformed shapes during curvilinear crack growth. Bulging caused by the applied pressure is observed. Moreover, severe flapping is predicted as the crack turns. Figure 23 shows the computed stress intensity factors and T-stress vs the half-crack extension at the right crack tip. The sign conventions of stress intensity factors follow those in Ref. 3. Predicted results suggest the following:

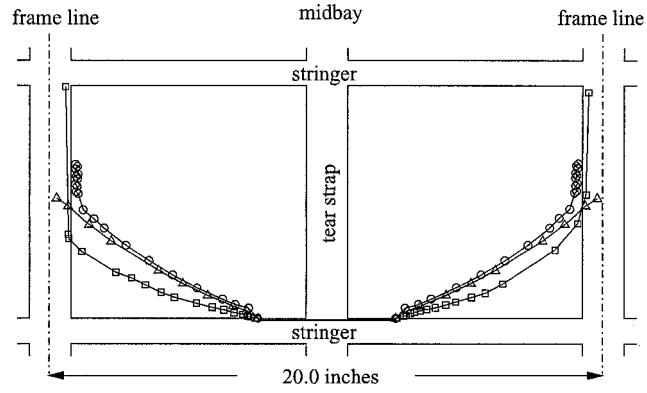

Fig. 21 Comparisons between predicted and measured crack trajectories (isotropic directional criterion with various magnitudes of r_c): □, measured; △, predicted (r_c = 0); and ○, predicted [r_c = 0.09 in. (2.29 mm)].

1) The T-stress has a very mild influence on the early crack trajectory prediction because of its relatively small magnitude. But as the crack approaches the tear strap, T-stress increases and plays an important role in the crack turning prediction. For the case with $r_c = 0.09$ in. (2.29 mm), a sharp turning caused by T-stress is predicted as the crack approaches the tear strap.

2) The computed fracture parameters for $r_c = 0$ and 0.09 in. (2.29 mm) are comparable at the early stage of curvilinear crack growth. However, sharp turning as the crack approaches the tear strap alters the deformation and stress fields. This drastically changes the computed values of fracture parameters.

Predicted crack paths from both numerical simulations at the right and left crack tips are almost symmetric about the midbay, but the measured crack paths are not. This observation gives a preliminary indication of the experimental scatter that might occur in the panel test.

2. Effect of Fracture Toughness Orthotropy

The predicted crack-growth trajectories depicted in Fig. 21 are comparable to the experimental measurements, but with some discrepancy. The disagreement during early stages of crack growth might be related to the fracture toughness orthotropy of the fuselage skins.

In subsequent analyses the orthotropic directional criterion, that is, Eq. (4), is used to predict the propagation angle. From the coupon test results the fracture toughness for this material and thickness is about 100 ksi $\sqrt{\text{in.}}$ (109 mPa $\sqrt{\text{m}}$) in the L direction and 105–120 ksi $\sqrt{\text{in.}}$ (114 mPa $\sqrt{\text{m}}$–131 mPa $\sqrt{\text{m}}$) in the T direction.[3] Thus, the fracture toughness is assumed to be 10% higher in the T than in the L direction. The predicted crack trajectories with $r_c = 0.09$ in. (2.29 mm) are compared with those from the isotropic prediction and experimental measurements. As shown in Fig. 24, during early stages of crack growth the predicted trajectories for the orthotropic case agree better with the experimental measurements than the isotropic case. Crack-growth simulation with fracture orthotropy also predicts crack turning as the crack approaches the tear strap. Yet, when the crack grows further into the tear strap region the inclusion of fracture orthotropy adversely alters the crack path prediction and does not predict flapping as observed in the panel test.

Several possible reasons might explain why the current methodology including the fracture toughness orthotropy does not predict the desired flapping and should be examined in future research:

1) A characteristic feature of fracture orthotropy in the tear strap region is that the material orientation in the tear strap differs from that in the skin (that is, the transverse direction in the tear strap is along the longitudinal direction of the skin and vice versa). As a

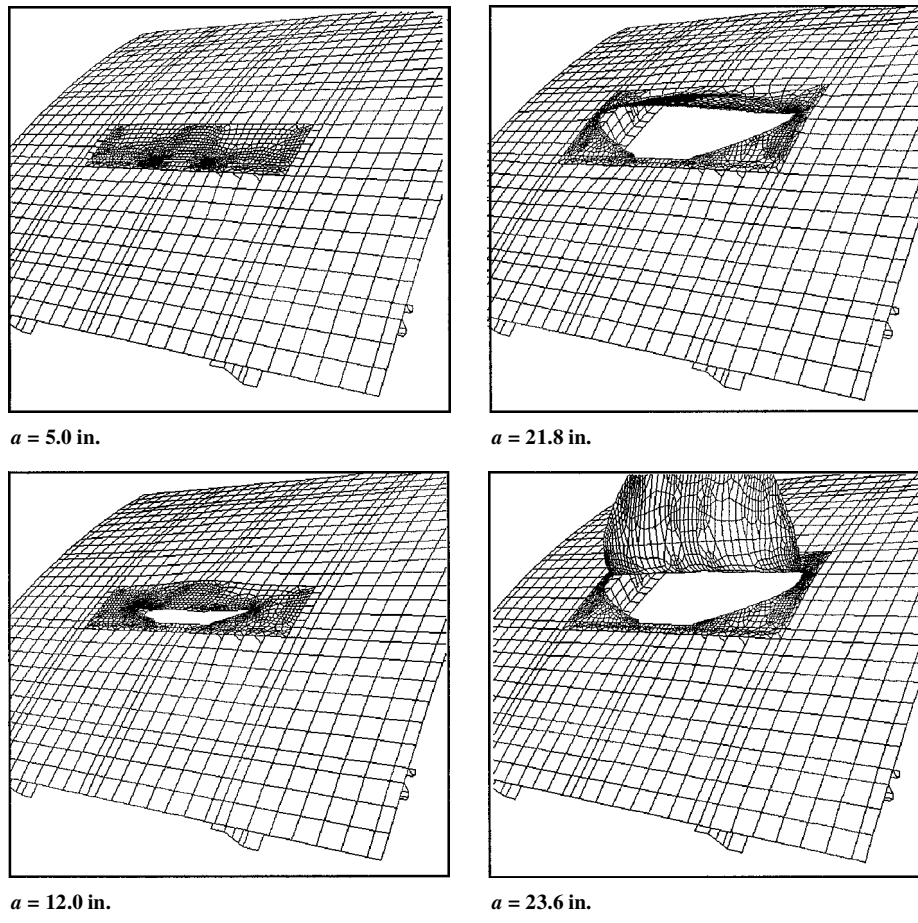

Fig. 22 Computed deformed shapes during curvilinear crack growth [isotropic case with $r_c = 0.09$ in. (2.29 mm), magnification factor = 2.0].

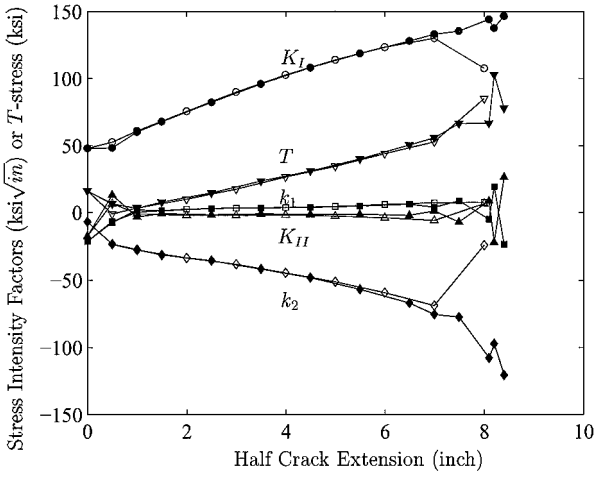

Fig. 23 Computed stress intensity factors and T-stress vs half-crack extension. The hollow and solid markers denote the computed fracture parameters for the isotropic case with $r_c = 0$ and 0.09 in. (2.29 mm), respectively.

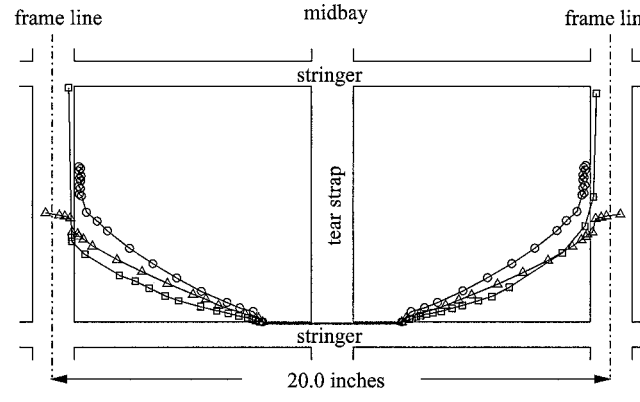

Fig. 24 Comparisons between predicted and measured crack trajectories [isotropic and orthotropic cases with $r_c = 0.09$ in. (2.29 mm)]: □, measured; ○, predicted (isotropic); and △, predicted (orthotropic, $K_c(T)/K_c(L) = 1.1$).

result, the material characteristics in this overlapped region might behave like a quasi-isotropic material with less fracture toughness orthotropy.

2) The skin and tear strap are assumed to be perfectly bonded in the current model. However, as the crack grows into this region the adhesive bond between the skin and tear strap is likely to fail. This inevitably alters the local crack-tip stress fields and consequently affects the crack-growth behavior.

3) The thin-shell approximation does not capture all of the three-dimensional complexities of the problem in the vicinity of the tear strap, particularly in the crack-tip region. Additional three-dimensional crack-growth simulations are needed to quantify the three-dimensional effect on crack turning prediction.

4) Accurate stress intensity factor and T-stress evaluations in this region are crucial to predict crack turning. Current crack-growth simulations use a low-order polynomial degree of shape functions for thin-shell finite element analyses and use a displacement correlation method to extract the T-stress term from the finite element solutions, which can be inaccurate. Other numerical methods, for example, path-independent integrals for geometrically nonlinear shells, should improve the accuracy of fracture parameter evaluations.

5) The crack-growth directional criterion and its subsequent curvilinear crack-growth simulations explicitly assume that the crack is grown under small-scale yielding conditions. Yet, as the length of the fatigue crack extends to tear strap, stable tearing and

extensive plasticity are likely to occur. The active plastic zone and accumulated plastic wake caused by stable tearing would likely affect the crack-growth prediction.

F. Comparisons with Previous Studies

Potyondy et al.[21] and Chen et al.[33] have reported numerical simulations for this problem previously. Both studies analyzed early curvilinear crack growth but did not address the issue of sharp turning as the crack approaches the tear strap. It is, nevertheless, of interest to compare these results with the current prediction.

In Potyondy et al.[21] and Chen et al.,[33] a global-local hierarchical modeling approach was used to model the panel test. Three hierarchical modeling levels were employed, composed of a global shell model, a 6×6 bay-stiffened panel model, and a 2×2 bay-stiffened panel model. Crack growth was only performed in the 2×2 bay model, the lowest level in the hierarchy. The kinematic boundary conditions on the 2×2 bay model were not updated during crack growth. Also, the boundary conditions applied to the global shell model corresponded with an open cylinder. Thus, the longitudinal stress in this numerical model is expected to be less than that in the test fixture because the test fixture is a closed cylinder.

The directional criterion used in Potyondy et al.[21] and Chen et al.[33] corresponds to the Erdogan and Sih directional criterion,[23] that is, Eq. (2); thus, comparisons are made with the isotropic prediction with $r_c = 0$. Figure 25 shows the predicted crack-growth trajectories from previous and current studies as well as experimental measurements. The initial crack location in Potyondy's simulations was modeled at 0.45 in. (11.43 mm) away from the intersection of the skin and stringer as a result of limitations in the previous version

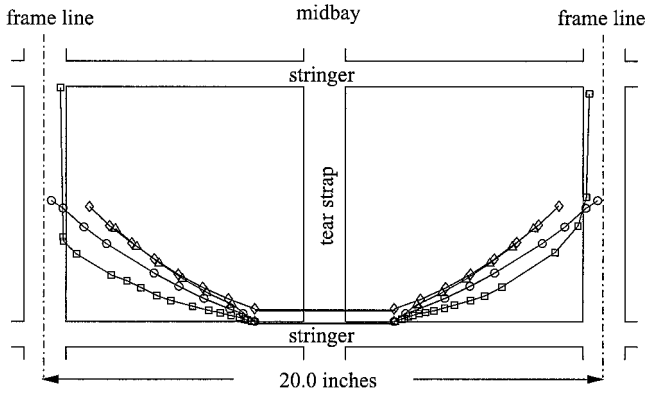

Fig. 25 Comparisons between predicted and measured crack trajectories (isotropic directional criterion with various magnitudes of r_c): □, measured; ○, predicted (current r_c = 0); △, predicted (Chen et al.[34]); and ◇, predicted (Potyondy et al.[21]).

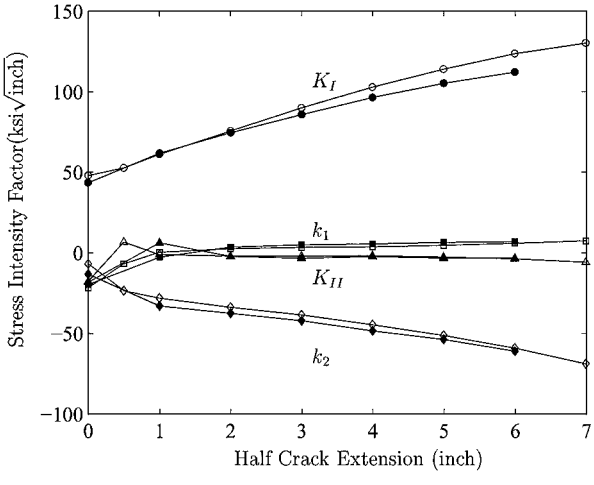

Fig. 26 Computed stress intensity factors vs half-crack extension. The hollow and solid markers denote the computed stress intensity factors from the current isotropic prediction with $r_c = 0$ and those from Chen et al.,[33] respectively.

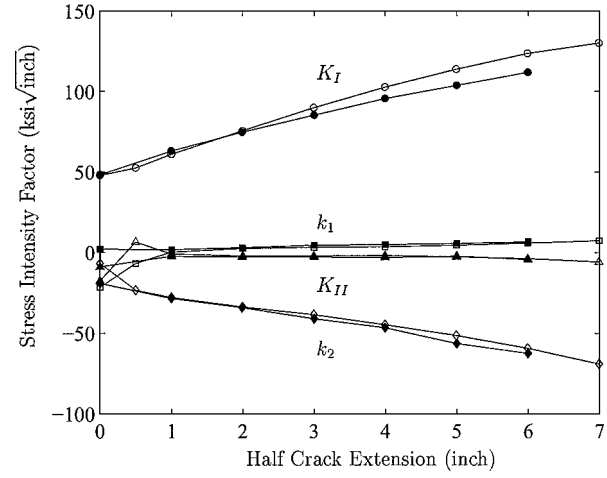

Fig. 27 Computed stress intensity factors vs half-crack extension. The hollow and solid markers denote the computed stress intensity factors from the current isotropic prediction with $r_c = 0$ and those from Potyondy et al.,[21] respectively.

of the FRANC3D program. Figures 26 and 27 show the computed stress intensity factors at the right crack tip in comparison with Potyondy et al.[21] and Chen et al.,[33] respectively. From these results one can conclude the following:

1) The applied axial force used to model the longitudinal stress caused by a closed cylinder has little influence on the computed stress intensity factors. This can be observed from the computed values shown in Fig. 26 at zero crack extension; the current model and the model used in Ref. 33 at this stage basically represent the same boundary conditions and crack configuration except an axial force was applied in the current model.

2) The fact that the kinematic boundary conditions were not altered during crack growth in the previous studies has a mild affect on the crack trajectory prediction and stress intensity factor computation. In the previous studies the kinematic boundary conditions used in the lowest level in the hierarchy were obtained from a global model with an initial 5.0-in. (127-mm) crack. The driving force for this case would be less than the one with updated boundary conditions as the crack grows. This is properly reflected on the computed K_I values shown both in Figs. 26 and 27. This seems to have little effect on the computed values of K_{II}, because they remain more or less the same for all cases. This leads to a lower ratio of K_{II}/K_I in the current model with updated boundary conditions. As a result, more shallow crack trajectories are predicted in the present study. Nevertheless, the computed fracture parameters are comparable with previous results; thus, a similar fatigue life is anticipated.

IV. Conclusions

The CTOA fracture criterion and elastic-plastic finite element analysis are used to predict fracture behavior and residual strength of KC-135 fuselage panels. The analysis methodology together with the FRANC3D/STAGS program is shown to be an effective tool to simulate 1) lead crack growth, 2) MSD crack growth, 3) multiple crack interaction, and 4) material thinning as a result of corrosion damage in pressurized fuselages.

In addition, curvilinear crack growth in a generic narrow-body fuselage is studied. Comparisons with experimental measurements suggest that the fracture toughness orthotropy plays an important role in predicting the early crack-growth trajectories. The subsequent crack growth after the initial crack deflection follows a trajectory where the local stress states are of a mode I dominant type. Thus, like crack growth in double cantilever beam specimens,[2] crack turning and flapping as the crack approaches the tear strap is highly related to the T-stress.

Acknowledgments

This work was performed with support from the NASA Langley Aircraft Structural Integrity Program under Contracts NAG-1-1184 and NAG-1-2069 and U.S. Air Force Corrosion Damage

Assessment Framework under Subcontract NCI-USAF-9128-001. The authors would like to thank James C. Newman Jr., David S. Dawicke, and Dale Cope for their support and encouragement. Helpful discussions with the members of the Cornell Fracture Group are also appreciated.

References

[1]Harris, C. E., Starnes, J., Jr., and Newman, J., Jr., "Analytical Methodology for Predicting the Onset of Predicting Widespread Fatigue Damage in Fuselage Structure," *Proceedings of the Federal Aviation Administration–NASA Symposium on the Continued Airworthiness of Aircraft Structures*, edited by C. A. Bigelow, National Technical Information Service, Springfield, VA, 1996, pp. 63–88.

[2]Chen, C.-S., "Crack Growth Simulation and Residual Strength Prediction in Thin Shell Structures," Ph.D. Dissertation, School of Civil and Environmental Engineering, Cornell Univ., Ithaca, NY, Jan. 1999.

[3]Potyondy, D. O., "A Methodology for Simulation of Curvilinear Crack Growth in Pressurized Shells," Ph.D. Dissertation, School of Civil and Environmental Engineering, Cornell Univ., Ithaca, NY, Aug. 1993.

[4]Carter, B. J., Chen, C.-S., Wawrzynek, P. A., and Ingraffea, A. R., "A Topology-Based System for Modeling 3D Crack Growth in Solid and Shell Structures," *Proceedings of the Ninth International Congress on Fracture, ICF9*, edited by B. L. Karihaloo et al., Elsevier Science, Sydney, Australia, 1997, pp. 1923–1934.

[5]Rankin, C. C., Brogan, F. A., Loden, W. A., and Cabiness, H. D., "STAGES User Manual Version 2.4," Lockheed Martin Missiles and Space Co., Inc., Advanced Technology Center, Palo Alto, CA, 1997.

[6]Cope, D., "Corrosion Damage Assessment Framework: Corrosion/Fatigue Effects on Structural Integrity," Boeing Defense and Space Group, TR D500-13008-1, Wichita, KS, 1998.

[7]Newman, J. C., Jr., "An Elastic-Plastic Finite Element Analysis of Crack Initiation, Stable Crack Growth, and Instability," *Fracture Mechanics: Fifteenth Symposium*, edited by R. J. Sanford, American Society for Testing and Materials, Philadelphia, 1984, pp. 93–117.

[8]Maclin, J. R., "Performance of Fuselage Pressure Structure," *1991 International Conference on Aging Aircraft and Structural Airworthiness*, edited by C. E. Harris, NASA CP 3160, 1991, pp. 67–74.

[9]Miller, M., Kaelber, K. N., and Worden, R. E., "Finite-Element Analysis of Pressure Vessel Panels," *Proceedings of the International Workshop on Structural Integrity of Aging Airplanes*, edited by S. N. Atluri, Atlanta Technology Publications, Atlanta, 1992, pp. 337–348.

[10]Pettit, R. G., Wang, J. J., and Toh, C., "Validated Feasibility Study of Integrally Stiffened Metallic Fuselage Panels for Reducing Manufacturing Costs," NASA CR-2000-209342, May 2000.

[11]Swift, T., "Fracture Analysis of Stiffened Structure," *Damage Tolerance of Metallic Structures: Analysis Methods and Application*, edited by J. B. Chang and J. L. Rudd, American Society for Testing and Materials, Philadelphia, 1984, pp. 69–107.

[12]Hom, C. L., and McMeeking, R. M., "Large Crack Tip Opening in Thin Elastic-Plastic Sheets," *International Journal of Fracture*, Vol. 45, No. 2, 1990, pp. 103–122.

[13]Newman, J. C., Jr., Dawicke, D. S., Sutton, M. A., and Bigelow, C. A., "A Fracture Criterion for Widespread Cracking in Thin-Sheet Aluminum Alloys," *International Committee on Aeronautical Fatigue, 17th Symposium*, edited by A. F. Blom, Engineering Materials Advisory Series, West Midlands, England, U.K., 1993, pp. 443–468.

[14]Dawicke, D. S., Newman, J. C., Jr., and Bigelow, C. A., "Three-Dimensional CTOA and Constraint Effects During Stable Tearing in a Thin-Sheet Material," *Fracture Mechanics*, Vol. 26, edited by W. G. Reuter et al., American Society for Testing and Materials, Philadelphia, 1995, pp. 223–242.

[15]Dawicke, D. S., Sutton, M. A., Newman, J. C., Jr., and Bigelow, C. A., "Measurement and Analysis of Critical CTOA for an Aluminum Alloy Sheet," *Fracture Mechanics*, Vol. 25, edited by F. Erdogan, American Society for Testing and Materials, Philadelphia, 1995, pp. 358–379.

[16]Dawicke, D. S., "Residual Strength Predictions Using a Crack Tip Opening Angle Criterion," *Proceedings of the Federal Aviation Administration–NASA Symposium on the Continued Airworthiness of Aircraft Structures*, edited by C. A. Bigelow, National Technical Information Service, Springfield, VA, 1996, pp. 555–566.

[17]Dawicke, D. S., and Newman, J. C., Jr., "Residual Strength Predictions for Multiple Site Damage Cracking Using a Three-Dimensional Analysis and a CTOA Criterion," *Fatigue and Fracture Mechanics*, Vol. 29, edited by T. L. Panontin and S. D. Sheppard, American Society for Testing and Materials, Philadelphia, 1999, pp. 815–829.

[18]Sun, C. T., and Su, X. M., "The Effect of Crack Interaction on Ductile Fracture," *Proceedings of the Federal Aviation Administration–NASA Symposium on the Continued Airworthiness of Aircraft Structures*, edited by C. A. Bigelow, National Technical Information Service, Springfield, VA, 1996, pp. 161–170.

[19]Chen, C.-S., Wawrzynek, P. A., and Ingraffea, A. R., "Elastic-Plastic Crack Growth Simulation and Residual Strength Prediction of Thin Plates with Single and Multiple Cracks," *Fatigue and Fracture Mechanics*, Vol. 29, edited by T. L. Panontin and S. D. Sheppard, American Society for Testing and Materials, Philadelphia, 1999, pp. 97–113.

[20]Nilsson, K.-F., "Influence of MSD Crack Pattern on the Residual Strength of Flat Stiffened Sheets," *Computational Mechanics*, Vol. 23, No. 1, 1999, pp. 39–52.

[21]Potyondy, D. O., Wawrzynek, P. A., and Ingraffea, A. R., "Discrete Crack Growth Analysis Methodology for Through Cracks in Pressurized Fuselage Structures," *International Journal for Numerical Methods in Engineering*, Vol. 38, No. 10, 1995, pp. 1611–1633.

[22]Zaal, K., "A Survey of Crack Path Stability Criteria and Their Application to Crack Flapping Phenomena in Stiffened Structures," Faculty of Aerospace Engineering, Delft Univ. of Technology, TR LR-681, Delft, The Netherlands, Sept. 1992.

[23]Erdogan, F., and Sih, G. C., "On the Crack Extension of Plates Under Plane Loading and Transverse Shear," *Journal of Basic Engineering*, Vol. 85, No. 4, 1963, pp. 519–527.

[24]Pettit, R. G., Chen, C.-S., Ingraffea, A. R., and Hui, C.-Y., "Process Zone Size Effects on Naturally Curving Cracks," *Engineering Fracture Mechanics*, Vol. 68, No. 10, 2001, pp. 1191–1205.

[25]Chen, C.-S., Krause, R., Pettit, R. G., Banks-Sills, L., and Ingraffea, A. R., "Numerical Assessment of T-Stress Computation Using a P-Version Finite Element Method," *International Journal of Fracture*, Vol. 107, No. 2, 2001, pp. 177–199.

[26]Williams, J. G., and Ewing, P. D., "Fracture Under Complex Stress—The Angled Crack Problem," *International Journal of Fracture*, Vol. 8, No. 4, 1972, pp. 441–446.

[27]Finnie, I., and Saith, A., "A Note on the Angled Crack Problem and the Directional Stability of Cracks," *International Journal of Fracture*, Vol. 9, 1973, pp. 484–486.

[28]Buczek, M. B., and Herakovich, C. T., "A Normal Stress Criterion for Crack Extension Direction in Orthotropic Composite Materials," *Journal of Composite Materials*, Vol. 19, No. 6, 1985, pp. 544–553.

[29]Boone, T. J., Wawrzynek, P. A., and Ingraffea, A. R., "Finite Element Modeling of Fracture Propagation in Orthotropic Materials," *Engineering Fracture Mechanics*, Vol. 26, No. 2, 1987, pp. 185–201.

[30]Viz, M. J., Potyondy, D. O., Zehnder, A. T., Rankin, C., and Riks, E., "Computation of Membrane and Bending Stress Intensity Factors for Thin, Cracked Plate," *International Journal of Fracture*, Vol. 72, 1995, pp. 21–38.

[31]Sutton, M. A., Zhao, W., Boone, M. L., Reynolds, A. P., and Dawicke, D. S., "Prediction of Crack Growth Direction for Mode I/II Loading Using Small-Scale Yielding and Void Initiation/Growth Concepts," *International Journal of Fracture*, Vol. 83, No. 3, 1997, pp. 275–290.

[32]Kfouri, A. P., "Some Evaluations of the Elastic T-term Using Eshelby's Method," *International Journal of Fracture*, Vol. 30, No. 4, 1986, pp. 301–315.

[33]Chen, C.-S., Wawrzynek, P. A., and Ingraffea, A. R., "Methodology for Fatigue Crack Growth and Residual Strength Prediction with Applications to Aircraft Fuselages," *Computational Mechanics*, Vol. 19, No. 6, 1997, pp. 527–532.

A. N. Palazotto
Associate Editor